

On the rate of descent of overflows

Peter D. Killworth

Southampton Oceanography Centre, Southampton, England, UK

Abstract. The path taken by dense turbulent outflows usually requires the numerical solution of along-flow equations for mass, tracers, and momentum and cannot easily be predicted. Instead, we consider the consequences of two simple assumptions. First, there is a quadratic turbulent bottom drag. Second, the outflow is assumed to be approximately in local equilibrium so that a best fit formula from atmospheric and ocean surface layer observations plus large-eddy simulations, used by *Zilitinkevich and Mironov* [1996], can be used to predict the local thickness. (No energy budget for turbulent bottom layers is known, which is a constant difficulty for numerical models of such layers.) The equilibrium solution is approximately equivalent, for most oceanic conditions, to a constant bulk Richardson or Froude number. It is shown that dense turbulent overflows follow a simple trajectory, in which the rate of depth increase is a constant, until the level of turbulence drops sufficiently that the equilibrium solution becomes invalid. This result is independent of the detailed thermodynamics, entrainment or detrainment, and the quadratic drag coefficient (but does depend on the assumption of quadratic drag). Trajectories for the major overflow regions give reasonable results when compared with the limited available data. An argument is given as to why entrainment should only occur over limited regions, with detrainment elsewhere.

1. Introduction

Dense turbulent overflows occur downstream of many sills and straits which separate ocean basins. They form an efficient way in which much of the hydraulically controlled water passing across the sill can make its way into the deep basin beyond, with far less mixing than would occur had the water passed directly into the interior of the basin by laminar advection. Thus they form part of the intricate mechanism whereby water masses are formed and obtain their properties.

Overflows were originally studied by simplified stream tube models [*Smuth*, 1975; *Killworth*, 1977], recently updated to include realistic topography by *Price and Baringer* [1994]. *Emms* [1998] casts some doubt on the validity of stream tube models for two reasons. First, it has long been known that the derivation of the stream tube equations omits an extra pressure gradient term (see *Alendal* [1995] for a discussion). *Emms* showed that steady subcritical flows are unstable with the inclusion of this extra term. Second, his numerical simulations suggested that the flow could not be considered as uniform laterally across the stream tube and that draining by Ekman layers would play an important role (as in laboratory experiments by *Lane-Serff and Baines* [2000]).

Stream tube models, while extremely useful for understanding mechanisms, are hard if not impossible to include in more complicated models of ocean circulation. These cannot easily “lose” or “gain” fluid from grid boxes, which is required if the stream tube is either to be initiated at a sill, or to detrain at its buoyancy level. They also, by their nature, can only entrain and so cannot be suitable for global-scale models. On the laboratory scale at least, there is considerable evidence

that dense bottom flows are unstable and shed eddies, breaking the slowly varying assumptions of stream tube theory [*Ertling et al.*, 2000].

These and other considerations led to the production of more general models, notably the two-dimensional model of *Jungclauss and Backhaus* [1994], which permitted lateral variation in the flow as well as splitting of the “tube” by topography [*Jungclauss et al.*, 1995]. In turn, these models provided partial impetus to the recent developments in bottom boundary codes for ocean models [e.g., *Beckmann and Döscher*, 1997; *Killworth and Edwards*, 1999; *Song and Chao*, 2000]. Such codes adopt partial or complete aspects of “slab” physics for a bottom boundary layer, and are now being actively examined to ascertain what degrees of improvement such models give to climate simulations [e.g., *Dengg et al.*, 1999]. The “slab” approach is generally necessary since the ocean interior, above the bottom layer, is described by rather coarse vertically resolved physics (typical grid spacings of 200 m or more), so that, rather as with atmospheric boundary layer studies, full progress is likely to be made only when resolution of the boundary layer and its vicinity becomes affordable. Another disadvantage of the “slab” approach is that, unlike the surface boundary layer which can gain or lose turbulent energy due to forcing, no energy equation is available for the bottom boundary layer (all available terms act as turbulent energy sources, so that the layer would apparently have to entrain everywhere). This has led to approaches varying from the layer having dynamics borrowed from the interior [*Beckmann and Döscher*, 1997] to the employment of an equilibrium turbulence solution from atmospheric, oceanic and large-eddy simulations to predict a slab depth [*Killworth and Edwards*, 1999]. This latter approach will be used here.

Other, non-slab, approaches are also being considered (*Hallberg*, personal communication, 2001), and process models using three-dimensional numerical codes have been car-

Copyright 2001 by the American Geophysical Union.

Paper number 2000JC000707
0148-0227/01/2000JC000707\$09.00

ried out [Jiang and Garwood, 1995]. To evaluate the effects of such parameterisations requires a variety of comparisons with the sketchy data available. While making global tests of variations on a modification of the Killworth and Edwards formulation [Nurser *et al.*, 2000], the path of the outflows became an object of study. Stream tube models predict the path, which is solved as one of a set of ordinary differential equations for momentum, tracers, etc. The purpose of this paper is to show that under fairly general circumstances (which include the local equilibrium formulation mentioned above for layer thickness, appearing as a constant Froude or Richardson number), the outflow path is simply described by the geometry of the topography and is otherwise independent of the physics of the outflow. This is derived (section 2) and briefly compared with data (section 3). A short discussion of entrainment and detrainment follows (section 4).

2. The Model

When a turbulent bottom flow has passed through a sill, it initially falls rapidly before turning under the action of Coriolis force. After approximately a deformation radius, the along-slope velocity has become almost exactly geostrophic [Price and Baringer, 1994; Emms, 1997]. At this stage the flow is almost along-slope and sinking at a small angle θ to the depth contours. There are three components to the force balance for small Rossby number. Two of these would occur under any model assumptions: Coriolis, oriented almost up-slope and normal to the flow, and gravity, oriented down-slope. The third relates solely to bottom drag. Within the assumption of a slab-like flow the drag can only appear as a body force. We follow the normal practice of modeling this as a quadratic term, divided by the layer depth to turn it into a body force.

Two balances can be obtained from the force balance. While formally valid only for stream tubes, they are sufficiently general to hold under much wider conditions (and certainly apply to extant bottom boundary codes). The first, and more usual, is along-flow geostrophy, which, unusually, is not used directly here but noted for later. Resolving the forces normal to the flow gives the familiar [Nof, 1983; Condie, 1995] along-flow geostrophic balance

$$fu = g' |\nabla D| \quad (1)$$

where f is the Coriolis parameter, u is the (almost) along-slope velocity, g' is the reduced gravity given by $g' = g(\rho_{\text{bottom}} - \rho_{\text{interior}})/\rho_0$, and $D(x, y)$ is the topography depth. This relation will only hold after the outflow has moved a distance of about a deformation radius (i.e., so that geostrophy has had time to hold).

The second balance is more relevant here. Resolving along the flow gives the frictional balance

$$g' |\nabla D| \theta = \frac{C_D \mu^2}{h} \quad (2)$$

where C_D is the quadratic drag coefficient and h is the layer thickness. Some evidence for the validity of this is given by the realistic stream tube results of Price and Baringer [1994], which use this balance.

An energy balance is needed. As noted in the introduction, no useful energy budget for a slab bottom boundary layer has as yet been produced. In particular, detrainment cannot occur

without a formulation for energy loss; a viable bottom boundary layer model must be able both to entrain and detrain. This forces the use of an alternative approach, and we follow Killworth and Edwards [1999] and use the local equilibrium solution of Zilitinkevich and Mironov [1996]. Those authors derived an expression predicting layer depth based on best fits to a wide variety of atmospheric and oceanic boundary layer observations, together with large eddy simulation numerical experiments. It is known [Killworth and Edwards, 1999] to fit the scant bottom boundary layer observations quite accurately, e.g., those of Armi and Millard [1976] and Baringer and Price [1997a].

We use here the slightly simplified form of the Zilitinkevich and Mironov [1996] local equilibrium solution, rewritten by Killworth and Edwards [1999] (see them for a discussion) as

$$\left(\frac{h}{C_n u_* f} \right)^2 + \frac{h}{C_D C_i^2 |\mathbf{u}|^2 / g'} = 1 \quad (3)$$

where u_* is the friction velocity, $C_n = 0.5$, and $C_i = 20$. (C_n and C_i are best fit constants defined by Zilitinkevich and Mironov; under some circumstances they might have weak variation with other aspects of the bottom boundary layer regime left unconsidered by Zilitinkevich and Mironov, e.g., bottom slope. They note that C_n , in particular, could use more rigorous evaluation, and we shall permit it to vary slightly in what follows.) Appendix A shows that the second term in (3) dominates the first save over very strongly sloping topography and modifies the theory slightly in such cases. As we shall see, however, the changes at their largest are quite small and often negligible, so that (3) reduces to a Froude number criterion

$$\frac{u^2}{g'h} = \frac{1}{C_i^2 C_D} \quad (4)$$

Opinions vary as to which form of Froude number is likely to be more relevant. The form (4) agrees both in form and numerically with Armi and Millard [1976], but Baringer and Price [1997a] prefer the velocity shear ∂u rather than the bottom layer velocity u in the Froude number (in most parts of the ocean with weak deep flow, the differences are minor).

If $C_D = 3 \times 10^{-3}$, as used by Killworth and Edwards [1999], then $u/\sqrt{(g'h)} = 0.9$ (rising to 1.1 if $C_D = 2 \times 10^{-3}$), which is in good agreement with results from the early part of the Mediterranean outflow [Baringer and Price, 1997a], though the later part has rather smaller values, suggesting that the mixing has ceased so that the Zilitinkevich and Mironov formula would cease to hold, a case discussed below. For comparison, Johnson *et al.* [1994] find a ratio of the squares of u_* and u (one measure of a drag coefficient) to be $2.5 (\pm 0.7) \times 10^{-3}$.

Let s be an along-stream variable. Then the rate of vertical descent along the slope is

$$\frac{dD}{ds} = \theta |\nabla D| = \frac{C_D \mu^2}{g'h} = C_D \frac{1}{C_i^2 C_D} = \frac{1}{C_i^2} = \frac{1}{400} \quad (5)$$

for the Zilitinkevich and Mironov values. It should be noted that this rate is independent of the drag coefficient (it is numerically similar to C_D only if the Froude number of the layer is near unity, which would not be the case if C_D were, for example, 10^{-3}). It should be noted that the Zilitinkevich and Mironov theory, couched in terms of friction velocity, can be thought of as including a quadratic drag law, so that an argu-

ment could be made that C_D "cancels out" within their theory. Certainly, such cancellation would not occur for any other drag law, although a quadratic is certainly the most realistic available.

The descent rate is also independent of the remainder of the dynamics and thermodynamics. For example, the layer may be either entraining or detraining, but (5) continues to hold. As a result, the path of the descent of the (center of the) overflow can be mapped without knowledge of other dynamics. In practice, if the overflow moves at an angle ϕ to the eastward direction (x , with coordinates x east y north),

$$\frac{dD}{ds} = D_\lambda \cos \phi + D_\lambda \sin \phi = |\nabla D| \cos(\phi - \lambda) = \frac{1}{C_i^2} \tag{6}$$

$$\phi = \lambda \pm \cos^{-1} \left(\frac{1}{C_i^2 |\nabla D|} \right)$$

where λ is the angle ∇D makes with the x axis. The sign of the solution to (6) depends on hemisphere.

The result (5) is the main result of this paper. Its independence of almost all quantities is surprising. Some theoretical confirmation is given by the plume studies of *Price and Baringer* [1994], in which they note that the trajectory of their plumes are unaffected by variations in initial conditions (though, of course, their dynamics did not include the Froude number criterion (4)).

The rate of descent predicted by (5) is an upper bound. If the turbulence level of the bottom layer decreases, both u and h decrease, and eventually the Froude number (4) predicts a very small thickness for the layer. In the *Killworth and Edwards* [1999] code the depth h has a minimum depth h_0 of 10 m, to which it is reset if it becomes lower. This is immediately equivalent to reducing the Froude number below its constant value. In this case, (2) predicts

$$|\nabla D| \theta = \frac{C_D \mu^2}{g' h_0}$$

and

$$h_0 > \frac{C_i^2 C_D \mu^2}{g'}$$

so that

$$\frac{dD}{ds} = |\nabla D| \theta < \frac{1}{C_i^2}, \tag{7}$$

showing that the rate of descent slows when the flow is less active. However, Ekman drainage could then take place, which would instead increase the rate of descent.

3. Results

The simple formula for rate of descent can be applied to the four main overflows in the Atlantic: the Gibraltar outflow, the

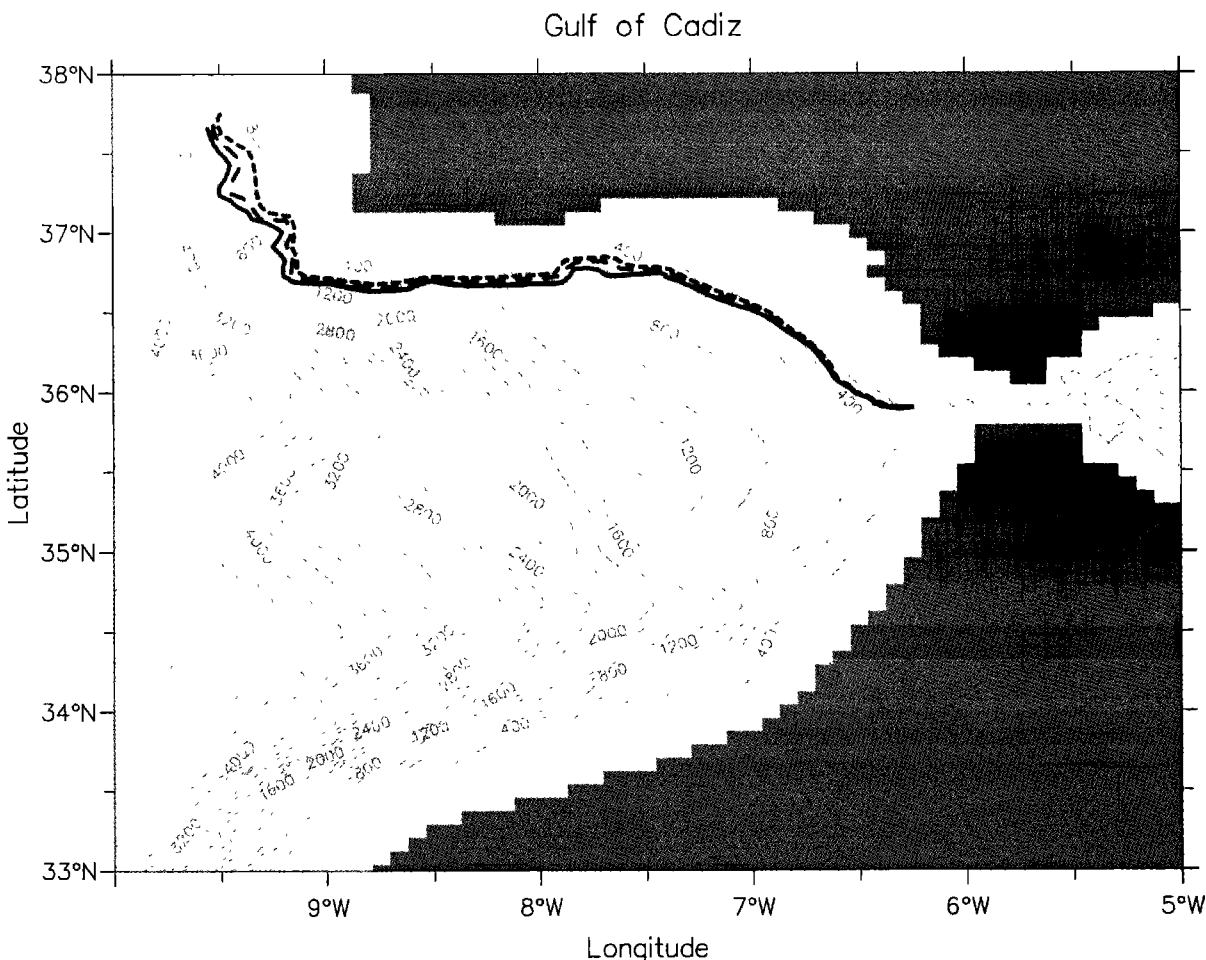


Figure 1. Predicted path of the Mediterranean outflow for descent rates 1/400 (thick solid line), 1/450 (long-dashed line), and 1/500 (short-dashed line). The topographic contour interval is 200 m.

Denmark Strait, the Faroe Bank Channel, and the Filchner Ice Shelf in the Weddell Sea, as discussed in much greater detail by *Price and Baringer* [1994]. The ETOPO5 topography [*National Geophysical Data Center*, 1988] was used, sometimes with smoothing on various length scales. Various choices were made for C , and hence for the rate of descent. From a chosen starting location, (6) provided the angle the trajectory made with the eastward direction (the calculation used spherical coordinates for accuracy), with a right or left choice depending on the sign of the Coriolis parameter. This was then expressed as the rate of change of longitude and latitude with along-stream distance, and these equations were integrated using an Adams method. In cases in which the local slope was smaller than the rate predicted by (5), the layer is assumed to descend along the maximum downward slope until the slope increased. In flatter topography, it can happen that a "bowl" is entered, from which the trajectory cannot escape; in such cases the trajectory is terminated. In such cases, the Froude number would earlier have fallen below its critical value, and such locations probably not reached. In addition, the extended formula for the rate of descent, valid when slopes become large, was also run; when this had a nonnegligible effect, this will be noted in what follows.

3.1. Gibraltar Outflow

Figure 1 shows the predicted path for the outflow, starting at the same location as used by *Price and Baringer's* [1994] stream tube model, using as rates of descent 1/400, 1/450, and 1/500. The three trajectories have very similar spatial locations, but of course, their depths vary. The trajectory agrees well with the stream tube model, to the extent of rounding Cape St. Vincent in a similar manner (although the outflow dynamics would probably have ceased by that time). The path predicted by using the full formula for descent rate (equation (A2)) with parameters equivalent to the 1/400 rate is fractionally deeper, as it must be, but its position is no farther from the unmodified result than are the differences between the 1/400 and 1/450 results.

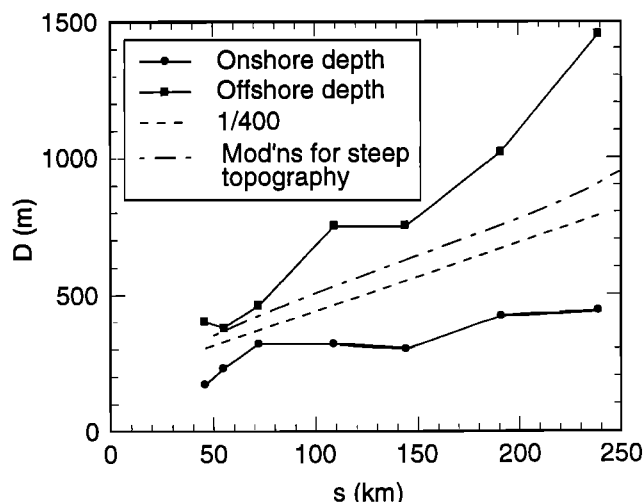


Figure 2. Predicted Mediterranean outflow depths as a function of along-outflow distance s using a constant descent rate of 1/400 (dashed line), compared with the on-shore and offshore depths observed by *Baringer and Price* [1997a]. Also shown (long- and short-dashed line) is the change made by using the full formula in Appendix A.

The predicted depth (for a descent rate of 1/400) is shown against *Baringer and Price's* [1997a] observations of on-shore and offshore depths of the outflow (their figure 8c) in Figure 2, and lies approximately halfway between the two bounds. (There appears to be some confusion as to precise locations and depths in the work of *Baringer and Price* [1997a, 1997b]. The distances between their sections in *Baringer and Price* [1997a, Figures 1 and 8] does not match that in *Baringer and Price* [1997b, Table 2]. Similarly, the depths shown in *Baringer and Price's* [1997a, Figures 1, 8 and 14] show differences. Defining these quantities, as they note, is far from easy. For consistency, their Figure 8 data have been used here.)

This is not a stringent test since (1) the mass-weighted transport is not necessarily halfway between the on-shore and offshore depths and (2) when the outflow width reaches around 50 km, for realistic bottom slopes this corresponds to a range of depths of several hundred meters. The only other easy comparison is with the *Price and Baringer* [1994] stream tube trajectory (their Figure 4), which is indistinguishable from that in Figure 1. At the simple level of this paper, the prediction of constant rate of fall is clearly working well. A further test is given by the long- and short-dashed line in Figure 2, which shows the changes made by using the full (A2) formula. This predicts a slightly deeper trajectory (as it must). Over the range shown, the two lines are almost parallel, ~ 100 m apart. There is little divergence between the two, probably because the majority of the effects of the full formula occurred in steeper topography near the start of the trajectory.

3.2. Denmark Strait

Figure 3 shows trajectories for rates of descent 1/400, 1/450, and 1/500 for a starting point at 65.8°N , 28.5°W . The topography here has been slightly smoothed from the original ETOPO5 data. The more rapid descent rates in this set have trajectories which leave the main slope at $\sim 39^\circ\text{W}$ and turn southward, eventually ending their trajectories in flatter basins; the slower descent trajectories are similar to the stream tube paths of *Price and Baringer's* [1994] Figure 8.

Comparison with data is less easy than for the Mediterranean since there are less surveys. *Saunders* [2000; Figure 4] survey shows a summary of paths of both Denmark Strait and Faroe Bank Channel overflows. The slower rate of descent trajectories (1/500 and 1/600; the latter is not shown) appear to fit his data better than the faster descent trajectories. This is especially true in the vicinity of Cape Farewell, where *Saunders* indicates a depth of ~ 2500 m: all trajectories are somewhat lower than this. However, other data suggest the outflow to be lower. Discovery Cruise 230 (S. Bacon, personal communication, 2000), part of which formed WOCE section A25, shows a depth of the core of the outflow at ~ 2500 m somewhat earlier, $\sim 62^\circ\text{N}$, and between 2500 and 3000 m southeast of Cape Farewell, at $\sim 42^\circ\text{W}$ (*Saunders* [2000] shows this section; see his Figure 11). The natural variability inherent in outflow paths makes direct comparison difficult, but the suggestion here is that the faster rates of descent (around 1/400) again fit at least some of the data. In such cases the continuation of the trajectories becomes unrealistic, so that turbulence levels would have to have dropped to low values south of $\sim 62^\circ\text{N}$.

A useful set of measurements for comparison are given by *Dickson and Brown* [1994], who estimate both depth of the outflow and its angle with the isobaths (θ) at three arrays

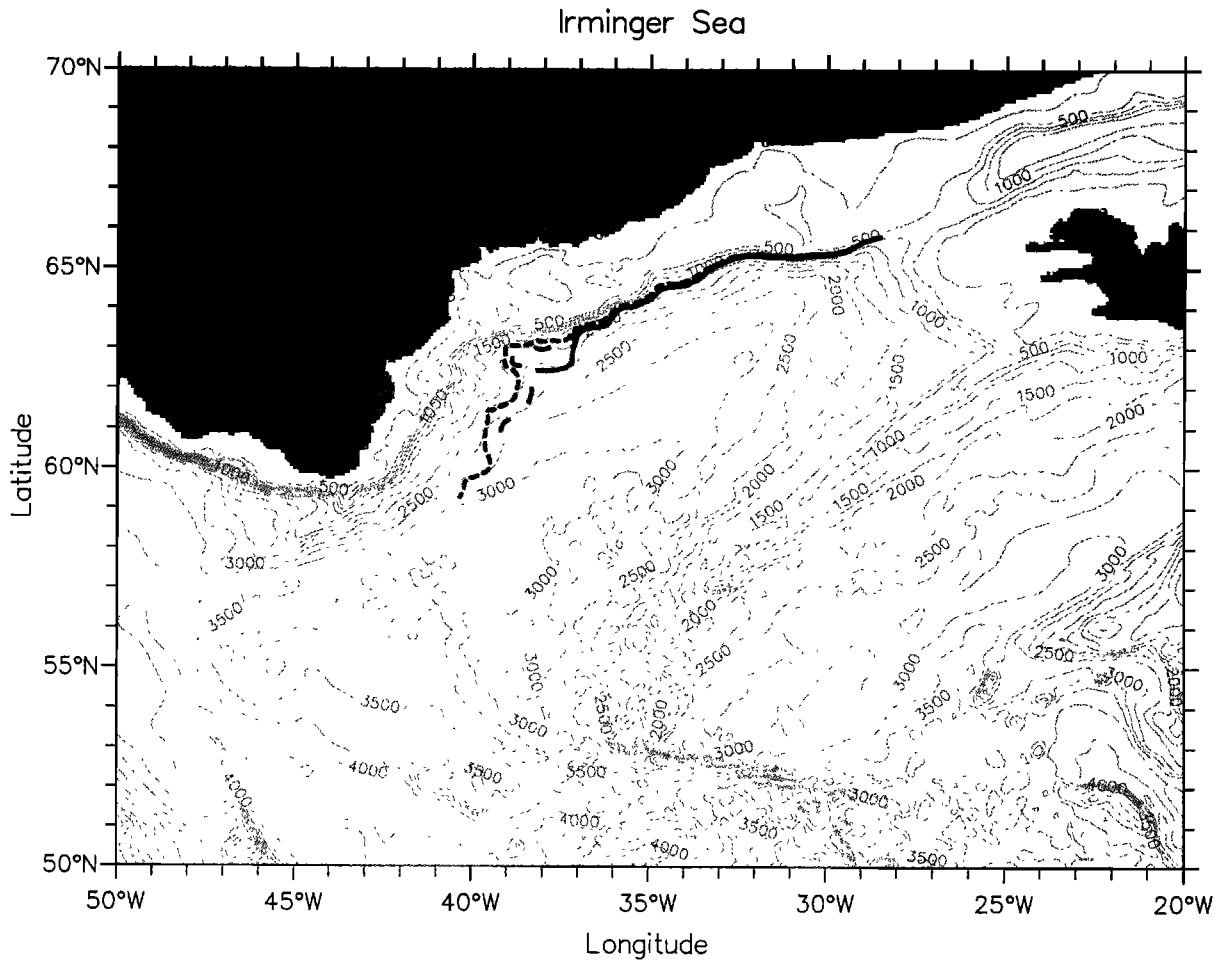


Figure 3. Predicted path of the Denmark Strait outflow, for descent rates 1/400 (thick solid line), 1/450 (long-dashed line), and 1/500 (short-dashed line). The topography has been slightly smoothed; contour interval is 250 m.

(Dohrn Bank, the Transient Tracers in the Ocean array, and Angmagssalik) as well as positioning the start of the outflow from 1973 data. The agreement with these data is shown in Figure 4. This shows the predicted depth of the outflow against Dickson and Brown's estimates (their Figure 12, in-

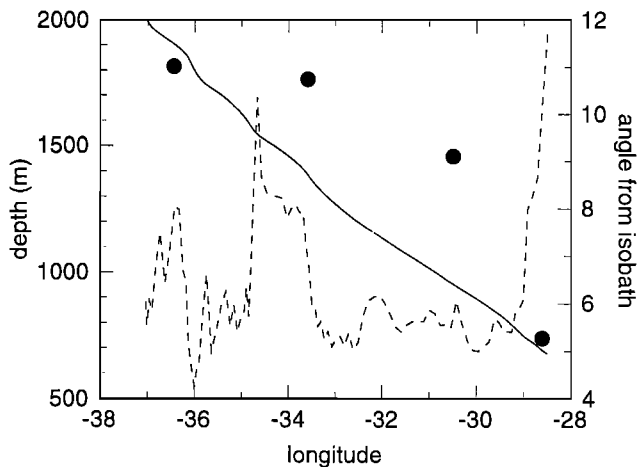


Figure 4. The depth of the Denmark Strait outflow (firm line, m) and the angle the flow makes with the isobath (degrees) for the 1/400 case in Figure 3. Solid circles show the estimates of core current depths from Dickson and Brown [1994].

dicated here by solid circles). The disagreement in the easternmost value is purely due to the slight differences in the topography used in our calculations. As the plume moves westward, it deepens at a roughly constant rate with longitude. This is clearly too shallow a descent between 34° and 30°W, but the depth at Angmagssalik (36.5°W) is well produced by the simple model. The dashed lines in Figure 4 show the angle of flow across the isobath in the model (which depends, of course, on the local topography). These can be compared with Dickson and Brown's [1994] estimates of mean values between the solid circles, which are (reading westward, i.e., from right to left in the diagram) 18°, 5°, and 4°. The model shows high values, up to 12°, near the initial outflow, dropping to around 5°, between the rightmost two circles, in rough agreement with but not as high as the 18° cited by Dickson and Brown. Interestingly, they suggest that this high angle is produced by entrainment, which is certainly taking place in reality in this area, whereas the simple model here can achieve high angles without requiring entrainment or detrainment to be occurring. Westward of this area, apart from a temporary increase to 10° near 34°W, values of θ lie around 5°, in good agreement with Dickson and Brown. Thus the model is capable of reproducing much of the observed behavior in the Denmark Strait overflow. Including the full (A2) formula produced no discernible changes to the simple 1/400 solution because the topography gradients are weak.

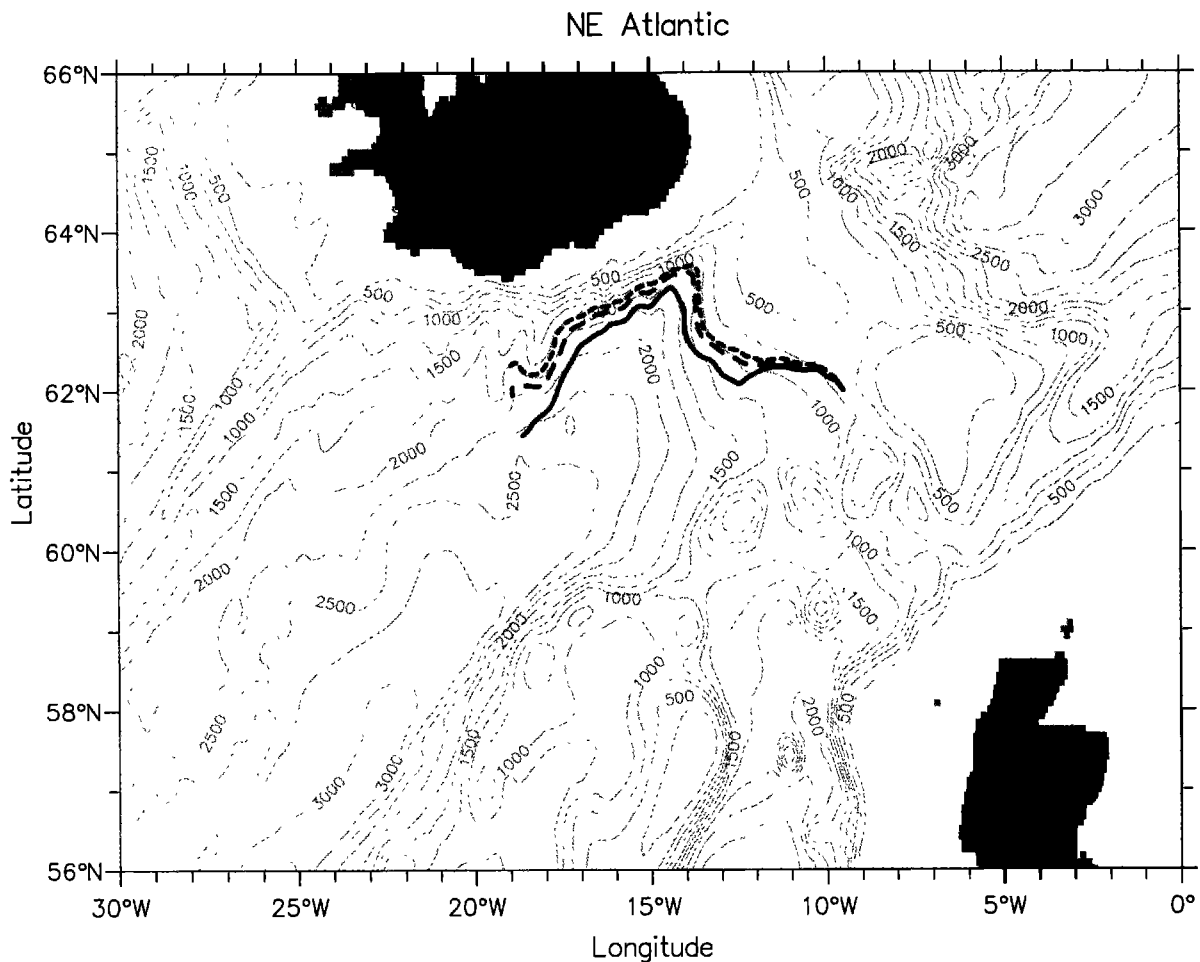


Figure 5. Predicted path of the Faroe Bank outflow, for descent rates 1/400 (thick solid line), 1/500 (long-dashed line), and 1/600 (short-dashed line). The topography has been slightly smoothed; contour interval is 250 m.

3.3. Faroe Bank Channel

Saunders [2000] also shows one section at $\sim 15^{\circ}$ – 17° W to indicate the path of the Faroe Bank Channel outflow, indicating a depth of the core of ~ 1400 m at a longitude of $\sim 17^{\circ}$ W. The trajectories in Figure 5 (for descent rates of 1/400, 1/500, and 1/600) suggest that the more rapid descent (1/400) is here not a good fit to the admittedly sparse data and that a slower rate, around 1/500, might be preferred. Indeed, all the trajectories fall somewhat below the stream tube predictions of *Price and Baringer* [1994, Figure 11]. However, the sparsity of data makes firm conclusions difficult. Again, including the full (A2) formula produced no noticeable changes to the simple 1/400 solution.

3.4. Filchner Ice Shelf

Offshore from the Filchner Depression is the main southern source of deep water. Measurements in this region are difficult due to ice, and the difficulties in retrieving current meter data can be summed up by noting that *Baines and Condie's* [1998] review of downslope flows only discusses conductivity-temperature-depth (CTD) data. Interpretation of such data is also not easy: *Foster and Carmack's* [1976] data shows bottom water at 3000 m as far east as 40° W.

Price and Baringer [1994] are again followed for a choice of starting point, which is here somewhat arbitrary. The initial

depth of the starting point is sensitive as to latitude because the slope is steep, as they note. However, the trajectories are again insensitive to initial details. Figure 6 shows trajectories for descent rates of 1/400, 1/450, and 1/500; at this scale they are almost indistinguishable. The trajectories are similar to that shown by *Price and Baringer* save that it reaches a depth of 3000 m somewhat earlier (*Price and Baringer's* trajectory having tended to follow depth contours in its later stages). No comparison with data can be made about which descent value is more accurate. Once more, including the full (A2) formula produced no discernible changes to the simple 1/400 solution.

4. Entrainment And Detrainment

The simple result above is independent of thermodynamics, which depend on whether the outflow is entraining or detraining and on how the reduced gravity g' changes along the trajectory. It is enlightening to extend slightly the arguments above to examine these effects. We neglect cabelling and other equation of state issues, which may be relevant in the Southern Ocean [*Killworth*, 1977].

Entrainment and detraining are handled in the *Killworth and Edwards* [1999] scheme by time stepping the equation for the layer depth h , velocity u (in fact both components, but we follow *Price and Baringer* [1994] here and ignore the small cross-stream component) and density ρ and then comparing

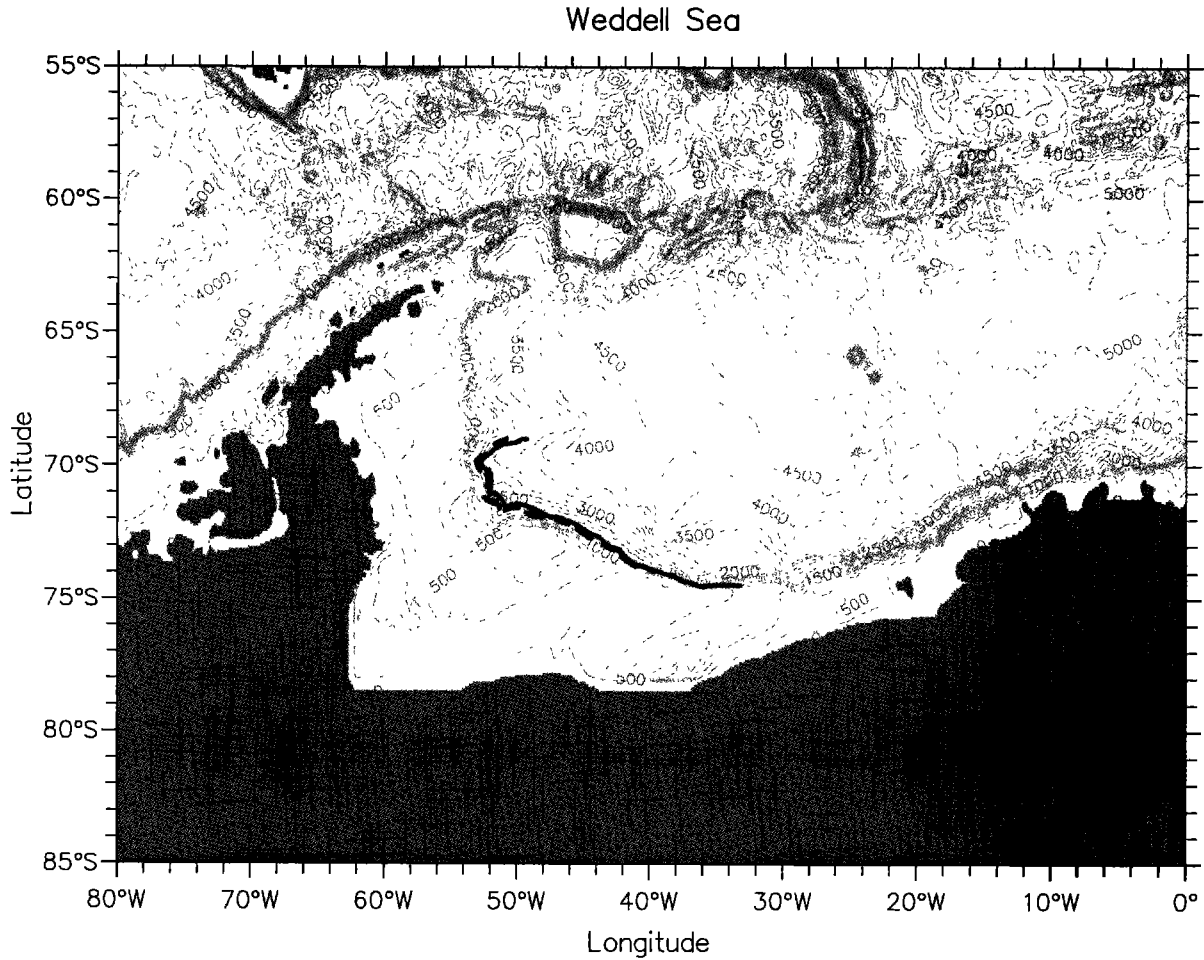


Figure 6. Predicted path of the Weddell Sea outflow, for descent rates 1/400 (thick solid line), 1/450 (long-dashed line), and 1/500 (short-dashed line). The topography has been slightly smoothed; contour interval is 250 m.

the predicted depth with the equilibrium solution given by (4). (The reader is reminded that no energy balance equation is known for a bottom boundary layer, implying an approach such as this.) If the predicted depth from the dynamical equations is larger than the equilibrium solution ($h_t > 0$), detrainment occurs as the depth is then reduced to its equilibrium depth; if the predicted depth is smaller than equilibrium ($h_t < 0$), entrainment occurs (and in this case interior fluid is mixed into the bottom layer, changing its properties). Note that the predicted changes are in the opposite direction to the physical description (i.e., in detrainment, h_t must be positive). If the flow is steady, then we can derive features of the solution very simply.

The depth and density satisfy conservation equations

$$h_t + (hu)_s = 0 \tag{8}$$

$$(hp)_t + (hup)_s = 0. \tag{9}$$

From these we may derive

$$\rho_t + u\rho_s = 0. \tag{10}$$

We now consider the cases of detrainment and entrainment separately.

4.1. Detrainment

In this case, (8) implies that the prediction for h_t is positive (so that h must be reduced to fit the local equilibrium solution). Thus, for detrainment,

$$(hu)_s < 0. \tag{11}$$

Since detrainment does not alter the layer values, requiring a steady state means that (10) implies

$$\rho_s = 0 \tag{12}$$

so that the layer density is not altered as the layer descends the slope. It therefore follows that the reduced gravity satisfies

$$g'_s = \frac{\partial}{\partial s} \left[\frac{g}{\rho_0} (\rho - \rho_l) \right] = \frac{g}{\rho_0} \frac{d\rho_l}{ds} = \frac{g}{\rho_0} \frac{d\rho_l}{dz} \frac{dz}{ds} = \frac{N^2(D)}{C_l^2} \tag{13}$$

where ρ_l is the undisturbed fluid density, the subscript l referring to interior, and N is the buoyancy frequency.

For consistency, (11) must be satisfied. By (1) and (4),

$$uh = \frac{C_l^2 C_D \mu^3}{g'} = \frac{C_l^2 C_D}{f^3} g'^2 |\nabla D|^3 \tag{14}$$

which must decrease along the trajectory. We have just seen that g' decreases monotonically. Under most conditions, dense outflows follow topography which, being concave, has a slope which decreases as the outflow falls downward. Thus both terms in (14) decrease along the trajectory and the assumption of detrainment is consistent. Only in regions in which the slope increases downwards will detrainment cease.

4.2. Entrainment

The prediction from (8) is now that h_i be negative, or

$$(hu)_i > 0. \quad (15)$$

Now, however, when local adjustment occurs, interior fluid is entrained; the net result is no temporal change of depth or density. The initial changes due to advection, then, satisfy

$$\delta h = -\delta t (hu), \quad (16)$$

$$\delta \rho = -\delta t u \rho_{,s}, \quad (17)$$

where the latter equation holds in any case. Mixing then occurs with the interior to remove the δh increment again, so that

$$(h + \delta h)(\rho + \delta \rho) + \rho_i(-\delta h) = \rho h \quad (18)$$

since the latter is the original undisturbed value. Thus

$$\rho \delta h + h \delta \rho - \rho_i \delta h = 0,$$

so that, after a little algebra,

$$(uh\rho)_{,s} = \rho_i(uh)_{,s}, \quad (19)$$

which is the standard entrainment algorithm, or using the definition of g' ,

$$(uhg')_{,s} = -uh \frac{N^2(-D)}{C_i^2}. \quad (20)$$

Using the definitions of u (1) and h (from (4)), this can be written entirely in terms of g' as

$$(g'^3 |\nabla D|^3)_{,s} = -g'^2 |\nabla D|^{3/2} \frac{N^2}{C_i^2}. \quad (21)$$

Requiring $(uh)_{,s}$ to be positive implies

$$(g'^2 |\nabla D|^3)_{,s} > 0. \quad (22)$$

It is clear that (21) implies that $(g'^3 |\nabla D|^3)$ decreases along the centerline of the fall, so that whether $(g'^2 |\nabla D|^3)$ can increase will depend on whether $|\nabla D|$ can increase sufficiently rapidly to counteract the rapid decrease of g' caused by entrainment. Under most circumstances one would have, for topography smoothed at least on the width of a typical outflow,

$$\frac{|\nabla D|_{,s}}{|\nabla D|} \ll \frac{|g'|_{,s}}{g'} \quad (23)$$

on simple geometric grounds, the simplest example of which would be constant slopes. If (23) is satisfied, $(uh)_{,s}$ cannot be positive, and so entrainment cannot occur.

This goes partway toward answering the question posed by *Price and Baringer* [1994], who wondered why entrainment was confined to relatively small areas in their integrations. To the extent to which the simple dynamics considered here holds, entrainment requires simultaneously rapid changes in topography and weak changes in reduced gravity; yet entrainment acts to ensure rapid changes in reduced gravity,

which is a partial contradiction. Thus this (slightly handwaving) argument confirms that entrainment is confined to small regions; under these dynamics, the majority of the flow is detrainment, however slightly.

5. Conclusion

We have shown one simple result: that the rate of descent of a dense slab-like overflow which is in local turbulent equilibrium with its surroundings will fall at a constant rate, independent of almost all environmental values (in particular, of bottom drag), for both entraining and detrainment flows. The predicted pathways of dense flows all seem plausible and in most cases consistent with a descent rate of around 1/400. This rate is also consistent with the dynamics used in the bottom boundary code of *Killworth and Edwards* [1999]. Data are frequently sparse, variable, or otherwise hard to interpret, and outflows can become quite wide and so occupy a large lateral extent; thus it is not easy to validate or disprove this simple result. However, there is good qualitative and quantitative agreement with observations in the Mediterranean outflow and west of Denmark Strait. The result cannot hold forever, and the outflow's rate of descent will probably slow when the local turbulence level drops below some minimum level.

Appendix A

We here show that for outflows, the second term in (3) dominates the first except in regions of strongly sloping topography and further show how to include it in such cases. Substituting $u_*^2 = C_D u^2$ and defining h from (2), (3) becomes

$$\frac{C_D u^2 f^2}{C_n^2 g'^2 |\nabla D|^2 \theta^2} + \frac{1}{|\nabla D| \theta C_i^2} = 1,$$

or, multiplying by $|\nabla D| \theta$ and using (1),

$$|\nabla D| \theta = \frac{1}{C_i^2} + \frac{C_D |\nabla D|^2}{C_n^2 |\nabla D| \theta}, \quad (A1)$$

where the terms are deliberately left in terms of the required quantity $|\nabla D| \theta$. If the first term on the right-hand-side of (A1) dominates we have the solution in the text. If the second term dominates, this would predict $|\nabla D| \theta = C_b^{1/2} |\nabla D| / C_n$. The ratio of this term to the original solution is

$$\frac{C_b^{1/2} |\nabla D| C_i^2}{C_n} \approx 44 |\nabla D|,$$

which is small for most topographic slopes although it could be important on some continental slopes. To include this term in calculations is trivial. (A1) is a quadratic for the rate of descent $|\nabla D| \theta$, with solution

$$|\nabla D| \theta = \frac{1}{2C_i^2} \left\{ 1 + \sqrt{(1 + 4\mu |\nabla D|^2)} \right\}, \quad (A2)$$

where $\mu = C_D C_i^4 / C_n^2$. (This reduces to the original formula when $44 |\nabla D|$ is small.) The change from the simple $1/C_i^2$ formula is monotonic, making the angle of fall slightly larger. However, tests in this paper show that the effects of this addition are negligible for the Denmark Strait and Faroe and Weddell Sea outflows and amount to a small offset for the majority of the Mediterranean outflow.

Notation

θ	angle of fall of outflow to depth contours.
f	Coriolis parameter.
u	along-slope velocity.
g'	reduced gravity.
D	topography depth.
C_D	quadratic drag coefficient.
h	layer thickness.
u_*	friction velocity.
C_n, C	universal constants defined by Zilitinkevich and Mironov [1996] (0.5, 20).
s	along-stream variable.
ϕ	angle of flow to eastwards direction.
x, y	axes east; north.
λ	angle ∇D makes with the x axis.
ρ	density.
t	time.
N	buoyancy frequency.
μ	nondimensional quantity ($C_D C_1^4 / C_n^2$).

Acknowledgements. Thanks to Jeff Blundell, who performed the integrations in this paper, and to Peter Saunders for reading it.

References

- Alendal, G., Solutions near the hydraulic control point in a gravity current model, *Phys Fluids*, 7, 2972-2977, 1995
- Armi, L., and R. C. Millard, The bottom boundary layer of the deep ocean, *J Geophys Res.*, 81, 4983-4990, 1976.
- Baines, P. G., and S. Condie, Observations and modelling of Antarctic downslope flows: a review, in *Ocean, Ice and Atmospheric Interactions at the Antarctic Continental Margin*, *Antarct Res Ser.*, vol. 75, pp. 29-50, AGU, Washington, D. C., 1998.
- Baringer, M. O., and J. F. Price, Mixing and spreading of the Mediterranean Outflow, *J. Phys. Oceanogr.*, 27, 1654-1677, 1997a.
- Baringer, M. O., and J. F. Price, Momentum and energy balance of the Mediterranean Outflow, *J. Phys. Oceanogr.*, 27, 1678-1692, 1997b.
- Beckmann, A., and R. Doscher, A method for improved representation of dense water spreading over topography in geopotential-coordinate models, *J. Phys. Oceanogr.*, 27, 581-591, 1997
- Condie, S. A., Descent of dense water masses along continental slopes, *J. Mar. Res.*, 53, 897-928, 1995
- Dengg, J., C. Boning, and U. Ernst, Effects of an improved model representation of overflow water on the subpolar North Atlantic, *Intl. WOCE Newsl.*, 37, 10-15, 1999.
- Dickson, R. R., and J. Brown, The production of North Atlantic Deep Water: Sources, rates, and pathways, *J. Geophys. Res.*, 99, 12,319-12,341, 1994.
- Emms, P. W., Streamtube models of gravity currents in the ocean, *Deep Sea Res., Part 1*, 44, 1575-1610, 1997.
- Emms, P. W., A streamtube model of rotating turbidity currents, *J. Mar. Res.*, 56, 41-74, 1998.
- Etling, D., F. Gelhardt, U. Schrader, F. Brennecke, G. Kühm, G. Chabert d'Hieres, and H. Didelle, Experiments with density currents on a sloping bottom in a rotating fluid, *Dyn. Atmos. Oceans*, 31, 139-164, 2000
- Foster, T. D., and E. C. Carmack, Frontal zone mixing and Antarctic Bottom Water formation in the southern Weddell Sea, *Deep Sea Res.*, 23, 285-300, 1976.
- Jiang, L., and R. W. Garwood Jr., A numerical study of three dimensional dense bottom plumes on a southern ocean continental slope, *J. Geophys. Res.*, 100, 18,471-18,488, 1995
- Johnson, G. C., T. B. Sanford, and M. O. Baringer, Stress on the Mediterranean Outflow plume, part I, Velocity and water property measurements, *J. Phys. Oceanogr.*, 24, 2072-2083, 1994.
- Jungclauss, J. H., and J. O. Backhaus, Application of a transient reduced gravity plume model to the Denmark Strait overflow, *J. Geophys. Res.*, 99, 12,375-12,396, 1994
- Jungclauss, J. H., J. O. Backhaus, and H. Fohrmann, Outflow of dense water from the Storfjord in Svalbard: A numerical model study, *J. Geophys. Res.*, 100, 24,719-24,728, 1995.
- Killworth, P. D., Mixing on the Weddell Sea continental slope, *Deep Sea Res.*, 24, 427-448, 1977
- Killworth, P. D., and N. R. Edwards, A turbulent bottom boundary layer code for use in numerical ocean models, *J. Phys. Oceanogr.*, 29, 1221-1238, 1999.
- Lane-Serff, G. F., and P. G. Baines, Eddy formation by overflows in stratified water, *J. Phys. Oceanogr.*, 30, 327-337, 2000.
- National Geophysical Data Center, Digital relief of the Surface of the Earth, Data Announcement 88-MGG-02, Natl. Geophys. Data Cent., NOAA, Boulder, Colo., 1988
- Nof, D., The translation of isolated eddies on a sloping bottom, *Deep Sea Res.*, 30, 171-192, 1983.
- Nurser, A. J. G., P. D. Killworth, and S. G. Alderson, A new approach to the sigma-coordinate pressure gradient problem in a terrain-following bottom boundary layer model, *Intl. WOCE Newsl.*, 39, 34-36, 2000
- Price, J. F., and M. O. Baringer, Outflows and deep water production by marginal seas, *Progr. Oceanogr.*, 33, 161-200, 1994.
- Saunders, P. M., The dense northern overflows, in *Ocean Circulation and Climate*, pp. 401-417, Academic, San Diego, Calif., 2000.
- Smith, P. C., A streamtube model for bottom boundary currents in the ocean, *Deep Sea Res.*, 22, 853-873, 1975
- Song, Y., and Y. Chao, An embedded bottom boundary layer formulation for z -coordinate ocean models, *J. Atmos. Ocean Technol.*, 17, 546-560, 2000
- Zilitinkevich, S., and D. V. Mironov, A multi-limit formulation for the equilibrium depth of a stably stratified boundary layer, *Boundary-Layer Meteorol.*, 81, 325-351, 1996.

P. D. Killworth, Southampton Oceanography Centre, Empress Dock, Southampton SO14 3ZH, England, UK. (e-mail: p.killworth@soc.soton.ac.uk)

(Received November 3, 2000; revised June 8, 2001; accepted July 5, 2001)